Closed-Loop Control of Deep Brain Stimulation: A Simulation Study

Sabato Santaniello, *Member, IEEE*, Giovanni Fiengo, *Member, IEEE*, Luigi Glielmo, *Senior Member, IEEE*, and Warren M. Grill, *Senior Member, IEEE*

***Abstract*—Deep brain stimulation (DBS) is an effective therapy to treat movement disorders including essential tremor, dystonia, and Parkinson's disease. Despite over a decade of clinical experience the mechanisms of DBS are still unclear, and this lack of understanding makes the selection of stimulation parameters quite challenging. The objective of this work was to develop a closed-loop control system that automatically adjusted the stimulation amplitude to reduce oscillatory neuronal activity, based on feedback of electrical signals recorded from the brain using the same electrode as implanted for stimulation. We simulated a population of 100 intrinsically active model neurons in the Vim thalamus, and the local field potentials (LFPs) generated by the population were used as the feedback (control) variable for closed loop control of DBS amplitude. Based on the correlation between the spectral content of the thalamic activity and tremor (Hua *et al.*, 1998), (Lenz *et al.*, 1988), we implemented an adaptive minimum variance controller to regulate the power spectrum of the simulated LFPs and restore the LFP power spectrum present under tremor conditions to a reference profile derived under tremor free conditions. The controller was based on a recursively identified autoregressive model (ARX) of the relationship between stimulation input and LFP output, and showed excellent performances in tracking the reference spectral features through selective changes in the theta (2–7 Hz), alpha (7–13 Hz), and beta (13–35 Hz) frequency ranges. Such changes reflected modifications in the firing patterns of the model neuronal population, and, differently from open-loop DBS, replaced the tremor-related pathological patterns with patterns similar to those simulated in tremor-free conditions. The closed-loop controller generated a LFP spectrum that approximated more closely the spectrum present in the tremor-free condition than did open loop fixed intensity stimulation and adapted to match the spectrum after a change in the neuronal oscillation frequency. This computational study suggests the feasibility of closed-loop control of DBS amplitude to regulate the spectrum of the local field potentials and thereby normalize the aberrant pattern of neuronal activity present in tremor.**

***Index Terms*—Autoregressive model (ARX), deep brain stimulation (DBS), essential tremor, local field potentials, minimum variance control, Parkinson's disease, recursive least-squares (RLS) identification.**

Manuscript received December 22, 2009; revised May 21, 2010; accepted August 16, 2010. Date of publication September 30, 2010; date of current version February 09, 2011.

S. Santaniello was with the Department of Engineering, Università del Sannio, 82100 Benevento, Italy, and the Department of Biomedical Engineering, Duke University, Durham, NC 27708 USA. He is now with the Department of Biomedical Engineering, Johns Hopkins University, Baltimore, MD 21218 USA (e-mail: ssantan5@jhu.edu).

G. Fiengo and L. Glielmo are with the Department of Engineering, Università del Sannio, 82100 Benevento, Italy (e-mail: gifiengo@unisannio.it; glielmo@unisannio.it).

W. M. Grill is with the Department of Biomedical Engineering, Duke University, Durham, NC 27708 USA (e-mail: warren.grill@duke.edu).

Digital Object Identifier 10.1109/TNSRE.2010.2081377

I. Introduction

DEEP brain stimulation (DBS) is an effective therapy to treat the symptoms of several movement disorders, including essential tremor (ET), Parkinson's disease (PD), and dystonia. DBS delivers high frequency ($\sim$130-185 Hz) pulse train stimulation to specific subcortical targets, including the subthalamic nucleus (STN), the internal segment of the globus pallidus (GPi), or the ventral intermediate nucleus (Vim) of the thalamus via a surgically implanted electrode and battery-powered implanted pulse generator [3]. Although DBS greatly reduces motor symptoms, limits drug-induced side effects, improves performance of activities of daily living, and enhances quality of life [3], the mechanisms of action of DBS remain uncertain [4].

This lack of understanding makes the selection of the stimulation parameters (i.e., voltage, pulse duration, and frequency), which are programmed by a clinician following implantation of the device, quite challenging. Experimental studies in ET [5], [6], PD [7], [8], and dystonia [9], [10] demonstrate that motor symptoms depend nonlinearly on the frequency and amplitude of stimulation. There are few guidelines available to guide the selection of appropriate stimulus parameters, and programming is largely an ad hoc process that relies on clinical expertise and does not necessarily result in optimal outcomes. As well, the selection of parameters has important implications for power consumption, and thus the battery life of the implanted pulse generator [11].

The long-term objective of our work is to develop a closed-loop control system that automatically adjusts the stimulation parameters to achieve reduction of motor symptoms based on feedback of electrical signals recorded from the brain using the same electrode as implanted for stimulation. The aims of the present study were to use computational modeling to design a closed-loop control system and determine the feasibility of feedback control of the power spectrum of the local field potentials (LFPs). We focused on DBS of the Vim for tremor suppression and developed an adaptive model-reference control scheme [12] based on the recursive identification of a model of neural activity in the thalamus during tremor. The extracellular LFPs resulting from the superposition of the aggregate activity of a population of model neurons around the electrode were used as a measure of the system state (i.e., amount of tremor). LFPs are an appropriate feedback signal as they can be readily measured using the clinically implanted DBS electrode [13], [14], and there is very high correlation between field potentials and

tremor in both ET and PD [1], [2]. Further, changes in the LFPs along the cortico–basal ganglia–thalamic motor loop are correlated with changes in motor symptoms [15], [16].

In a computer simulation, we implemented a closed-loop controller to modulate the neuronal activity by application of extracellular stimulation, and the neuronal activity was related to the input (electrical stimulus) through a reduced-order linear autoregressive input-output model [17]. Based on the identified input-output model, a feedback control law was designed to restore tremor-free conditions, i.e., modify the electrical activity of the neurons in the target site such that the simulated LFPs exhibited spectral properties akin to those observed in tremor-free conditions [18], [19].

II. Methods

We simulated a population of independent, noncommunicating model neurons to determine the effects of extracellular stimulation on neuronal activity and to calculate the extracellular local field potentials generated by the active neurons in tremor and tremor-free conditions. Subsequently, the relationship between the applied stimulus current (input) and the LFPs (output) was modeled with an ARX (autoregressive with exogenous input) difference equation with parameters identified using the minimum-prediction-error approach [17]. A minimum variance control algorithm was then implemented to regulate the spectral character of the LFPs by altering the stimulation intensity in the tremor condition according to a reference spectrum from the tremor-free condition.

A. Simulation of the Evoked Local Field Potentials

One hundred model thalamocortical (TC) relay neurons were uniformly distributed within 3 mm of a point source electrode positioned in an infinite homogeneous isotropic medium (resistivity $\rho = 500\ \Omega\mathrm{cm}$, [20]). The model neurons had a multicompartment structure, with explicit geometrical representation of the dendrites, cell body, and myelinated axon, and a full complement of nonlinear ionic membrane conductances, which replicate a broad complement of the electrophysiological properties of TC relay neurons [21]. Results obtained in previous instantiations of populations of the same model neurons correlated exceedingly well with changes in tremor from human subjects during DBS with different patterns, rates, and intensities of stimulation [22], [23].

Neuronal stimulation was determined using a two-step approach. First, the extracellular potentials generated by the electrode when the stimulus was ON were calculated [24]

$$V_{k,h}(t) = \frac{\rho \cdot I_{\mathrm{ext}}(t)}{4\pi \cdot r_{k,h}(P_{\mathrm{elc}})} \tag{1}$$

where $V_{k,h}(t)$ is the extracellular potential generated outside the hth compartment of the kth neuron at time t from the current $I_{\mathrm{ext}}(t)$ delivered by the electrode, and $r_{k,h}(P_{\mathrm{elc}})$ is the absolute distance of such compartment from the position P_{elc} of the point source electrode. Then, potentials $V_{k,h}(t)$ were applied and the neuronal response was computed by numerical integration using the CVODE method (time step $= 0.02$ ms). Simulations were implemented and run in NEURON, ver. 6.1 [25].

The extracellular LFPs generated by neuronal activity were calculated as the superposition of the potentials resulting from transmembrane currents in each neuronal compartment [24], [26]. At any point P and time t, the LFP was computed as

$$\phi(P,t) = \sum_{k=1}^{N} \sum_{h=1}^{l} \frac{\rho \cdot I_{k,h}(t)}{4\pi \cdot r_{k,h}(P)} \tag{2}$$

where $I_{k,h}(t)$ is the net transmembrane current in the hth compartment of the kth neuron at time t, $r_{k,h}(P)$ is the absolute distance of such compartment from the position P of the recording electrode, N is the number of neurons, and l is the number of compartments for each neuron. The small transmembrane currents flowing through the high impedance myelinated internodes were not included in the computation of the LFPs to reduce the computational effort. Field potentials were computed at three randomly selected points, all 2 mm from the center of the population (i.e., from the point source stimulating electrode), and were sampled at 25 kHz.

Simulations were repeated on three independently randomized neural populations. All analysis and signal processing was conducted in MATLAB (Mathworks, Natick, MA).

B. Simulation of Neuronal Activity Under Tremor-Free Conditions

We simulated the neuronal activity across a population of thalamic neurons in the absence of tremor, and we used this activity to develop a reference spectrum for subsequent closed-loop control. Based on single unit recordings from patients with chronic pain (no tremor reported) [18], we implemented four different spiking patterns, which reproduced the most prominent characteristics of the measured neuronal activity including multifarious spiking and bursting [18], [27]. Following the functional classification in [18] and the multiunit analysis in [28], 98 of the 100 neurons in each population were divided into two groups, with different average intrinsic firing rates: 74% "kinesthetic" (i.e., their firing rate was responsive to passive, imposed joint movements) and 26% "voluntary" (i.e., their firing rate was responsive to voluntary active joint movements). For each group, neurons were further classified as "regular," "random," or "irregular" according to the specific type of firing pattern they exhibited (definitions in [18]). The two remaining neurons exhibited irregular bursting activity [19] attributed to low-threshold calcium spikes (LTS). The intrinsic firing activity in the regular, random, irregular, and bursting neurons was simulated as follows (Fig. 1).

1) Regular: A binomial process with probability of success $p = 0.8$ was run at an average firing frequency of 19 Hz for voluntary cells (7 cells) and 16.1 Hz for kinesthetic cells (5 cells) [18]. When the output was 1, a spike was generated in the neuron by delivering a suprathreshold intracellular stimulus to the soma.

2) Irregular: Interspike intervals (ISIs) were drawn from an Erlang distribution with mean $\pm$ standard deviation equal to 19 ± 8.9 Hz for voluntary cells (16 cells) and 16.1 ± 8.5 Hz for kinesthetic cells (4 cells) [18]. When an ISI expired, a spike (and depending on the state of the neuron, sometimes two spikes) was

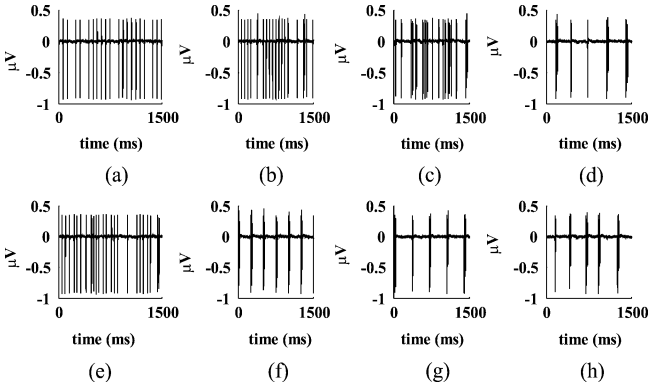

Fig. 1. Example of simulated patterns of neuronal activity under tremor-free (top row) and tremor (bottom row) conditions. Top row, from (a) to (d): extracellular evoked potentials from single kinesthetic regular, random, irregular, and bursting neurons. Bottom row, from (e) to (h): extracellular evoked potentials from single sporadic, tremor-locked, rhythmic (LTS), and random (LTS) bursting cells.

generated in the neuron by delivering a suprathreshold intracellular stimulus to the soma.

3) Random: A Poisson process $(\lambda = 1)$ was run at an average firing frequency of 19 Hz for voluntary cells (50 cells) and 16.1 Hz for kinesthetic cells (16 cells) [18]. For each newly drawn value ζ of the process, a pulse of current was delivered to the neuron. The duration d of the pulse was proportional to ζ according to an empirical rule $d = 8\zeta$ ms, and the amplitude was suprathreshold. This rule was chosen to produce a random bursting firing pattern, and it was noted in simulation that a suprathreshold stimulus to the soma of duration d resulted in a single burst of about ζ spikes.

4) Bursting: In two cells we sought to match the pattern of bursting described in [28], i.e., a weakly bimodal ISI histogram with a group of ISIs around 200–300 ms (see below). Interspike intervals were drawn from an Erlang distribution with mean $\pm$ standard deviation equal to 3.7 ± 0.6 Hz [28]. When an ISI expired, at least two spikes (and depending on the state of the neuron, sometimes three or more spikes) were generated in the neuron by delivering a suprathreshold intracellular stimulus of 15 ms to the soma.

Since there is no information regarding the spatial distribution of neurons from the different classes, a uniform distribution of each class in the 3-mm-radius sphere was assumed. Finally, random initial delays, uniformly distributed between 1 and 4 ms, were applied to the intracellular stimuli described above to increase variability among neurons, and white noise (mean $\mu = 0$ nA, variance $\sigma^2 = 3$ nA^2) was injected into the soma to simulate background synaptic activity [29].

C. Simulation of Neuronal Activity During Tremor

Similarly, we implemented four different patterns of firing activity across neurons in the modeled populations to simulate the intrinsic activity of thalamic neurons in persons with tremor. We chose the patterns to reproduce the primary statistical features (average firing rate, variance, and temporal distribution of spikes) of each type of thalamic neuron [28].

1) Sporadic: Fifty neurons were subjected to a sequence of 10-ms pulses of suprathreshold intracellular current with the interpulse intervals distributed according to an Erlang function with mean $\pm$ standard deviation of 14 ± 19 Hz [28], resulting in irregular firing of single or pairs of spikes.

2) Random (LTS) Bursting: Eleven neurons were subjected to a sequence of 15-ms pulses of suprathreshold intracellular current with the interpulse intervals distributed according to an Erlang function with mean $\pm$ standard deviation of 3.7 ± 0.6 Hz [28] resulting in two or three spike bursts and a weakly bimodal distribution of ISIs.

3) Rhythmic (LTS) Bursting: Five neurons were subjected to 20-ms pulses of suprathreshold intracellular current at a constant frequency. For each of them, the frequency was randomly drawn from a uniform distribution of 2–6 Hz and resulted in a periodic bursting activity for the neuron (each burst consisted of 3–5 spikes).

4) Tremor-Locked Bursting: Thirty-four neurons were subjected to 30-ms pulses of suprathreshold intracellular current at a frequency of 4 Hz [2] that resulted in periodic bursting activity.

The interburst intervals and proportion of neurons in each group were faithful to the experimental data [28]. Intraburst features (average firing rate: 235 Hz, range: 115–322 Hz [23]) were within the ranges provided in [28], but not faithful to the experimental data. This, however, has limited impact on the primary oscillations of the LFPs at frequencies below 100 Hz. As in the tremor-free case, neurons in different classes were randomly distributed in space and were subjected to both random delays in the timing of injected currents and noise.

D. Identification of the Input-Output Relationship

The relationship between the DBS stimulus (input) and LFPs (output) was identified using an ARX model. The input and output signals were low pass filtered (8-th order Butterworth filter, cutoff frequency: 100 Hz), down-sampled to $f_s = 1250$ Hz, and de-trended. We used the model structure

$$y(k) = \sum_{s=0}^{nb-1} b_s u(k-s-1) - \sum_{j=1}^{na} a_j y(k-j) + \varepsilon(k) \quad (3)$$

or, equivalently [17]

$$A(z^{-1})y(k) = B(z^{-1})u(k-1) + \varepsilon(k) \quad (4)$$

$A(z^{-1}) = 1 + a_1 z^{-1} + \cdots + a_{na} z^{-na}$, $B(z^{-1}) = b_0 + \cdots + b_{nb-1} z^{-nb+1}$ are polynomials in the Z-domain with na and nb to be chosen, $u(k)$ and $y(k)$ are the DBS stimulus and the recorded LFP at time kT, respectively, and T is the sampling interval $(T = 1/f_s = 0.8$ ms). Coefficients a_j, $j = 1, \ldots, na$ and b_s, $s = 0, \ldots, nb-1$ weight the linear dependence of the output at time kT on the previous na output samples and the last nb input values, respectively. $\varepsilon(k)$ represents unmodeled dynamics and is assumed to be white noise with mean 0 and variance ψ^2 to be estimated. We introduced the mean square prediction error

$$J = E\left[\left(\hat{y}(k|k-1) - y(k)\right)^2\right] \quad (5)$$

where $E[\cdot]$ is the expectation operator and $\hat{y}(k|k-1)$ is the prediction of the output at time k based on the knowledge of the actual value up to time $k-1$, i.e., from (4)

$$\hat{y}(k|k-1) = \left(1 - A\left(z^{-1}\right)\right) y(k) + B\left(z^{-1}\right) u(k-1). \quad (6)$$

The model parameters in (4) were identified in the following three different conditions by minimizing the prediction error (5) via a recursive least-squares (RLS) algorithm [17].

1) Tremor-free: The LFPs were calculated in the absence of tremor as described in Section II-B. Since no extracellular stimulus was applied, the ARX structure reduced to the AR structure [17]

$$A\left(z^{-1}\right) y(k) = \varepsilon(k). \quad (7)$$

2) Tremor with NO DBS: The LFPs were calculated during tremor as described in Section II-C, and since no stimulus was applied, the AR structure was used for identification.

3) Tremor with DBS ON: The LFPs were recorded during tremor as described in Section II-C, and fixed extracellular stimulation was applied to the population. The stimulus was a sequence of 100 μs cathodic current pulses with varying amplitudes (selected uniformly from values required to excite 10%, 30%, 50%, 70%, and 90% of the neurons) and instantaneous frequencies (selected uniformly from 10, 35, 60, 90, 130, and 185 Hz). This input was intended to probe the principal dynamics of the input–output relationship across both effective and ineffective stimulation settings [23] and provide a model of the plant for the subsequent design of the feedback controller.

In each of the three conditions, the recorded signals were split into two segments, one for identification (65% of the length) and the other for validation (35% of the length). The tremor-free and tremor with NO DBS conditions used 1 s trials and the DBS ON conditions used 10 s trials. Several model orders na and nb were tested, and we selected $na = 6$ and $nb = 1$ because such a choice provided a good fit to the available data and the power of the prediction differed from that of the validation data by less than 1%, independent of the position where the LFPs were recorded and of the neural population.

E. Approach to Feedback Control

The feedback controller aimed to modify the amplitude of the stimulus that was delivered to the neural population such that the tremor-related oscillations in the power spectrum of the LFPs were suppressed and the main features of the power spectrum of the LFPs calculated during the tremor-free condition were restored. The stimulation frequency was fixed at 130 Hz (aliasing-free, effective value). A generalized minimum variance control law [12] was designed based on the identified AR/ARX models, i.e., the control input $u(k)$ was computed by minimizing the variance of the modified tracking error

$$u(k) = \arg\left(\min_{u \in U} E\left[\left(P\left(z^{-1}\right) y(k+1) + Q\left(z^{-1}\right) u(k) - r(k)\right)^2\right]\right) \quad (8)$$

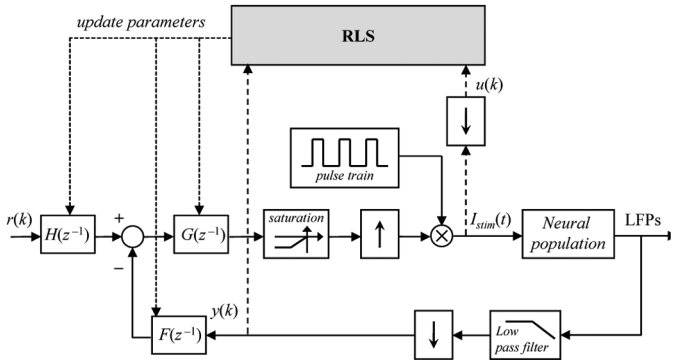

Fig. 2. Adaptive minimum variance control scheme. Local field potentials (LFPs) are low-pass filtered, sampled and fed back. The reference signal $r(k)$ and filtered LFPs $y(k)$ are processed to generate the control input. The extracellular stimulus $I_{\mathrm{stim}}(t)$ is obtained by multiplying the output of the controller by a pulse train. The stimulus is cathodic and the maximum amplitude allowed is 4.5 mA. $\uparrow=$ upsampling. $\downarrow=$ downsampling. RLS = identification procedure using the recursive least squares algorithm.

$\forall k \geq 0$, where U is the domain of the input amplitude (cathodic amplitudes limited to 4.5 mA, which was approximately the current required to activate 90% of the population) and the reference signal, $r(k)$, was obtained from the LFPs recorded in tremor-free conditions (Section II-B). In particular, the LFPs were low-pass filtered (cutoff frequency: 100 Hz), divided into consecutive 250 ms segments, and the individual segments were averaged. $P\left(z^{-1}\right)$ and $Q\left(z^{-1}\right)$ were chosen to guarantee a desired closed loop transfer function $T\left(z^{-1}\right)$ from the reference $r(k)$ to the output $y(k)$ (model reference control), thus forcing the output LFPs to reproduce the main spectral components of $r(k)$. The cost function in (8) weighted the tracking error between a filtered realization of the output signal $y(k)$ and the reference $r(k)$ (i.e., $P\left(z^{-1}\right) y(k+1) - r(k)$), wherein the filter depends on the desired closed-loop behavior, and the control effort $u(k)$. As in [12], we fixed $T(z^{-1}) = M_N\left(z^{-1}\right)/M_D\left(z^{-1}\right)$, the polynomials

$$\begin{aligned} M_N\left(z^{-1}\right) &= \gamma_0 + \gamma_1 z^{-1} + \cdots + \gamma_{n_N} z^{-n_N} \\ M_D\left(z^{-1}\right) &= 1 + \delta_1 z^{-1} + \cdots + \delta_{n_D} z^{-n_D} \end{aligned} \quad (9)$$

orders n_N, n_D, and parameters γ_i, $i = 0, \ldots, n_N$, and δ_j, $j = 1, \ldots, n_D$. Then, we designed $P\left(z^{-1}\right)$ and $Q\left(z^{-1}\right)$ as

$$\begin{aligned} P\left(z^{-1}\right) &= \frac{M_D\left(z^{-1}\right)}{M_N\left(z^{-1}\right)} - A\left(z^{-1}\right)\left(\frac{1}{\gamma_0} - 1\right) \\ Q\left(z^{-1}\right) &= B\left(z^{-1}\right)\left(\frac{1}{\gamma_0} - 1\right) \end{aligned} \quad (10)$$

with $A\left(z^{-1}\right)$ and $B\left(z^{-1}\right)$ from (4).

A block diagram of the feedback controller is shown in Fig. 2, where the transfer functions in the Z domain $F\left(z^{-1}\right)$, $G\left(z^{-1}\right)$, and $H\left(z^{-1}\right)$ minimize the function in (8) [12] and are given by

$$\begin{aligned} F\left(z^{-1}\right) &= z\left(M_D\left(z^{-1}\right) - \frac{A\left(z^{-1}\right) M_N\left(z^{-1}\right)}{\gamma_0}\right) \\ G\left(z^{-1}\right) &= \frac{\gamma_0}{M_N\left(z^{-1}\right) B\left(z^{-1}\right)} \\ H\left(z^{-1}\right) &= M_N\left(z^{-1}\right). \end{aligned} \quad (11)$$

$T(z^{-1}) = M_N\left(z^{-1}\right)/M_D\left(z^{-1}\right)$ was a second-order filter with bandwidth $[19,\ 45]$ Hz and gain 0.2. The design of $T\left(z^{-1}\right)$ was based on the analysis of the LFPs simulated in tremor-free conditions (Section III-A), and was intended to attenuate the low frequency components (< 7 Hz) of the closed loop system while amplifying the spectrum of $r\,(k)$ in the range 15–50 Hz. The choice of γ_0 influenced the weight of $u\,(k)$ in the cost (8) and indirectly impacted the performances of the control scheme.

The controller was adaptive and at each time step the coefficients of $A\left(z^{-1}\right)$ and $B\left(z^{-1}\right)$ in (11) were recursively updated via the RLS algorithm before a new value for the stimulus was computed. These results were compared to a fixed minimum variance control law, i.e., the controller used the same reference model $T\left(z^{-1}\right)$ but the coefficients of $A\left(z^{-1}\right)$ and $B\left(z^{-1}\right)$ in (11) were computed off line (Section II-D) and were not updated during the controller evaluation.

III. Results

We simulated the neuronal activity around the DBS electrode in tremor and tremor-free conditions by implementing model neurons with different firing patterns (Fig. 1) and randomizing their positions within the volume. Under tremor-free conditions, the LFPs had low amplitude and a dominant oscillation between 15 and 20 Hz, i.e., the average firing frequencies of the voluntary and kinesthetic neurons, respectively. In tremor conditions, tremor-locked bursting cells dominated the LFPs, generating a main rhythm at ~ 4 Hz. Such features were captured by the identified AR/ARX models and exploited in the closed loop control strategy to eliminate the tremor-related oscillations.

A. Simulated LFPs

A population of one hundred intrinsically active model neurons, randomly distributed within a 3-mm-radius sphere, was used to simulate the extracellular LFPs. The superposition of activity from the modeled neurons generated field potentials that exhibited distinct characteristics in the absence and presence of tremor. Under tremor-free conditions the LFP signal had low amplitude as a result of the asynchronous activity across the population of neurons [Fig. 3(a)]. The power spectrum revealed that the bulk of the signal power was between 10 and 20 Hz [Fig. 3(c)], consistent with the average firing rate of the voluntary and kinesthetic neurons. The additional peaks in the power spectrum, between 20 and 50 Hz, were due to the secondary harmonics of the main mode and the effects of convolution by the Hann window used to compute the power spectrum (Welch's method). The LFPs during tremor [Fig. 3(b)] were characterized by strong periodic increases in amplitude at the tremor frequency (i.e., 4 Hz) arising from the superposition of bursting activity of the tremor cells, which fired at the same frequency and with a small constant delay from one another. The power spectrum exhibited a broad peak, centered at the tremor frequency, and the signal content decreased rapidly above 10 Hz [Fig. 3(c)].

B. Identification of an Input–Output Model

The relationship between the stimulus (input) and LFPs (output) was identified using an autoregressive model. The temporal and spectral results of the identification procedure

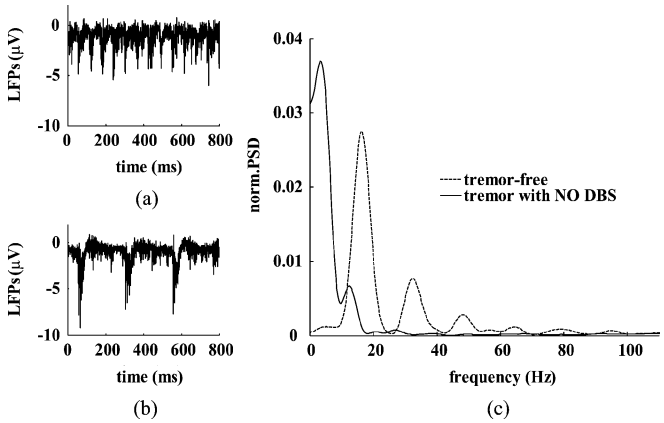

Fig. 3. Properties of the LFPs with NO DBS. Time pattern of the LFPs in the tremor-free (a) and tremor (b) conditions. (c) Normalized power spectral density (PSD) of the LFPs under tremor-free and tremor conditions obtained by dividing the PSD by the total computed power. LFPs in (a) and (b) were low-pass filtered, down-sampled and detrended to compute the PSDs in (c) using Welch's method with period of 250 ms (Hann window applied).

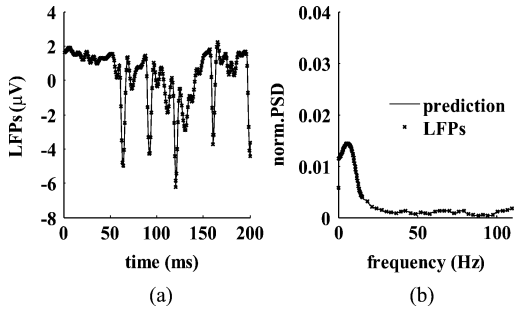

Fig. 4. Properties of the LFPs with DBS ON. Time pattern (a) and PSD (b) of the LFPs in the tremor condition with DBS ON and the one-step ahead prediction given by the identified ARX model ($na = 6,\ nb = 1$). PSD computation and normalization methods were as in Fig. 3.

are shown in Fig. 4 for one of the simulated neural populations in the tremor condition with DBS ON. The time pattern [Fig. 4(a)] and the power spectral density (PSD) [Fig. 4(b)] of the validation data set were compared with those of the one-step ahead prediction obtained using the ARX model (6). The prediction tracked the validation data very well (average rms error $= 8.6 \cdot 10^{-5}$) confirming that the model captured the primary dynamics of the available data. Similar results were achieved under the tremor-free condition (average rms error $= 2.3 \cdot 10^{-5}$) and the tremor condition with NO DBS (average rms error $= 3.0 \cdot 10^{-5}$).

The Bode plots of the identified input-output models under the tremor-free (AR), tremor with NO DBS (AR), and tremor with DBS ON (ARX) conditions (Section II-D) are shown in Fig. 5. The magnitude of the tremor-free transfer function was flat below $\sim$40 Hz with a small attenuation in the upper gamma range (50–70 Hz) and a small resonant peak at $\sim$100 Hz. The phase diagram was flat below $\sim$10 Hz and then declined almost linearly up to $\sim$100 Hz, thus causing phase distortion at low frequencies but not affecting harmonics in the beta (13–35 Hz) and gamma (50–70 Hz) ranges, where a linear phase delay was introduced. The phase at frequencies > 100 Hz was of minor concern since the corresponding gain was quite low. The tremor present

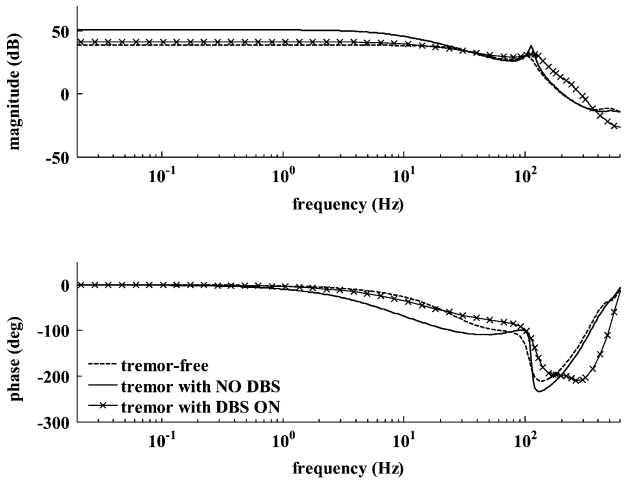

Fig. 5. Bode diagrams of the $\varepsilon - y$ transfer function obtained from the AR/ARX models identified on the LFPs in the tremor-free, tremor with NO DBS, and tremor with DBS ON conditions.

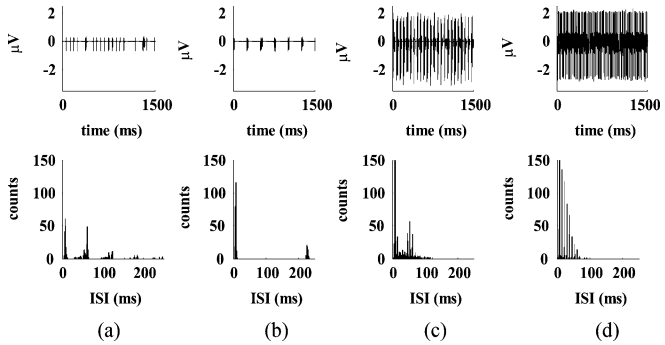

Fig. 6. Simulated patterns of neuronal activity represented as time series (top row) and interspike interval distribution (bottom row) under several conditions. (a) and (b): tremor-free (kinesthetic random firing) and tremor (tremor-locked bursting) conditions. (c): tremor conditions as in (b) with application of the closed-loop DBS. (d): tremor conditions as in (b) with application of open-loop, regular DBS (i.e., fixed amplitude $= -4.8$ mA, fixed frequency$= 130$ Hz). Histograms in (c) and (d) are truncated. Histograms constructed from 30 s simulations.

(NO DBS) transfer function had larger magnitude (~ 15 dB) than the tremor-free transfer function in the low frequency range and a marked phase lag from 2 to 100 Hz, thus amplifying the tremor-related activity and distorting oscillations in the other ranges. Finally, the transfer function of the autoregressive part of the identified ARX model in the tremor condition with DBS ON was similar to the tremor-free case, suggesting that the stimulation might mask the tremor-related activity by exciting other intrinsic dynamics.

These results suggested that the LFPs in tremor and tremor-free conditions were structurally different: the former exhibited a bursting profile with spectral content focused in the theta and alpha bands, while the latter exhibited tonic spiking and spectral components with a wider frequency range. This was confirmed by the substantial independence of the transfer function on the location where the LFPs were recorded: the variance of the ε-y transfer function computed over three different positions was close to 0 and the recording location did not affect its filtering properties.

The ARX model for the case of tremor with DBS ON, on the other hand, suggested that the LFPs depended almost linearly on the applied input, provided that suprathreshold stimuli were used. Moreover, since $nb = 1$, the model population responded to the background noise $\varepsilon(k)$ and the control input $u(k)$ in a very similar way. The transfer functions for the tremor condition with DBS ON and the tremor-free condition were almost coincident up to 100 Hz (Fig. 5), with minor differences in the high frequency range due to the applied input $u(k)$. The flat shape of the magnitude plot (Fig. 5) may account for the lack of tremor suppression by DBS when the stimulation frequency is < 100 Hz [5].

C. Feedback Control

The application of DBS, with amplitude determined by the adaptive feedback controller, modified the firing patterns of individual neurons, and this was reflected in the simulated LFPs as suppression of the characteristics associated with tremor and restoration of the spectral features present in the tremor-free condition. At the cellular level, stimulation altered the average firing rate and generated patterns of spiking similar to those in the tremor-free condition. This is shown in Fig. 6: a single model neuron, with a random kinesthetic firing pattern [Fig. 6(a)], fired short bursts of 2–3 spikes each (average intraburst ISI duration 7 ms) repeated quite regularly (inter-burst ISI ~ 63 ms). Such a pattern was dominant in the model population in the tremor-free condition, but was strongly altered in the tremor condition. In the tremor condition, longer bursts were noted with short intraburst ISIs [peak at 8 ms, Fig. 6(b)] and an inter-burst frequency ~ 4.5 Hz (inter-burst ISIs were in the range 219–233 ms with peak at 226 ms). The application of closed-loop DBS in the tremor condition elicited short bursts of 3–4 spikes, repeated once every ~ 54 ms (range 45–62 ms), and synchronized the firing activity across neurons to generate larger amplitude extracellular evoked potentials than in the case of tremor with NO DBS [Fig. 6(c), top]. Thus, closed-loop DBS appeared to mask the intrinsic low-frequency bursting activity and restore the primary rhythm of the kinesthetic firing pattern [Fig. 6(c), bottom]. In contrast, open-loop DBS (i.e., fixed amplitude and frequency) masked the intrinsic firing pattern by introducing sustained firing at the stimulation frequency [130 Hz in Fig. 6(d)], which suppressed the tremor-locked pattern but did not restore the oscillations observed in the tremor-free condition (more than 93% of all ISIs were shorter than 45 ms).

The effects of DBS on neuronal firing were similar across all patterns of intrinsic activity described in Section II-B and II-C, and led to consistent changes in the spectrum of the LFPs (Fig. 7). The reference input $r(k)$, which was an average version of the signal in Fig. 3(a), paced the model population via its main oscillation at ~ 20 Hz, while the feedback information was used to update the stimulus amplitude based on the detection of tremor-locked bursts. Finally, through the choice of the ratio $M_N\left(z^{-1}\right)/M_D\left(z^{-1}\right)$, the model-reference approach increased the gain of the closed-loop system to input harmonics in the alpha and beta bands. As a consequence, the controlled stimulus $I_{\mathrm{stim}}(t)$ exhibited a burst-like pattern as its amplitude

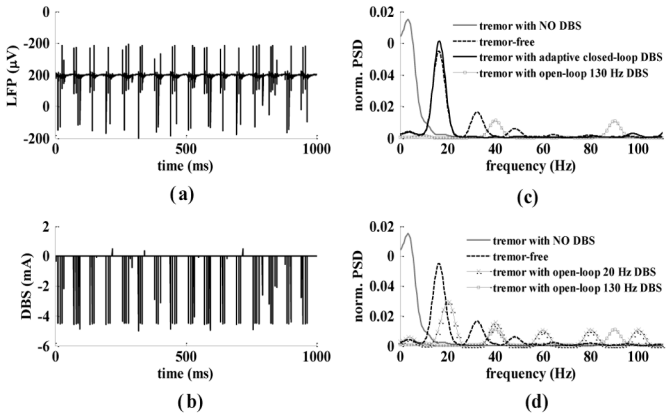

Fig. 7. Properties of the LFPs in the tremor condition with closed-loop DBS (a) and feedback controlled stimulation amplitude $I_{\mathrm{stim}}(t)$ (b) generated by the proposed control scheme. (c) Normalized PSD of the LFPs in the tremor-free condition, in the tremor condition with NO DBS, in the tremor condition with closed-loop DBS, and in the tremor condition with open-loop (130 Hz) DBS. (d) Normalized PSD of the LFPs in the tremor condition with NO DBS and in the tremor condition with low (20 Hz) and high (130 Hz) frequency open-loop DBS. 130 Hz open-loop DBS was as in Fig. 6(d). PSD computation and normalization methods in (c) and (d) were as in Fig. 3. DBS amplitude is limited as in Fig. 2.

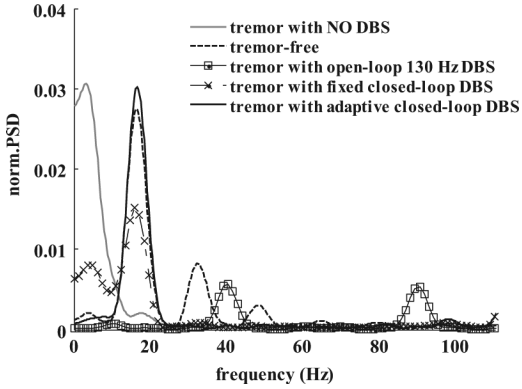

Fig. 8. Normalized power spectral density of the LFPs in the tremor-free condition, in the tremor condition with NO DBS, in the tremor condition with open-loop 130 Hz DBS, in the tremor condition with closed-loop adaptive DBS, and in the tremor condition with fixed closed-loop DBS. The firing pattern of the tremor-locked cells was modified to elicit bursts at an average frequency of 1 Hz. PSD computation and normalization methods were as in Fig. 3.

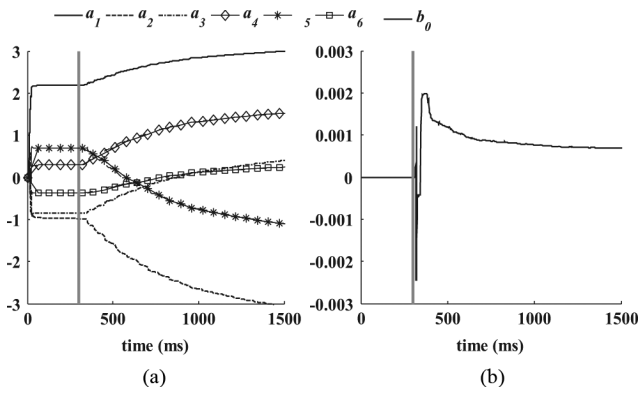

Fig. 9. Recursive estimation of the parameters of $A(z^{-1})$ (a) and $B(z^{-1})$ (b) in (4) ($na = 6$, $nb = 1$) during closed-loop adaptive stimulation in the tremor condition. The firing pattern of the tremor-locked cells was as in Fig. 8. DBS was turned ON at time $t = 300$ ms (grey line), after the model neurons had reached steady state firing patterns. Initial values of the parameters were 0.

was modulated to adapt the stimulus to the current state of the LFPs [Fig. 7(b)].

The normalized PSD of the LFPs across the four conditions is depicted in Fig. 7(c): the controller restored the characteristics of the tremor-free spectrum by reducing dramatically the power in the tremor (i.e., theta) band $[2,\ 7]$ Hz and amplifying the harmonics in the alpha and beta ranges. The power spectra further revealed dramatic differences between open- and closed-loop DBS: both approaches reduced the spectral content in the range $[2,\ 7]$ Hz, but open loop stimulation also reduced power at the intermediate frequencies and introduced a new high-frequency component at the stimulation frequency, while closed-loop DBS restored the primary peaks of the spectrum present in the tremor-free condition. An additional comparison was conducted with open-loop low frequency (20 Hz) DBS [Fig. 7(d)]: although the frequency of stimulation was close to the main rhythm of the signal in tremor-free conditions [Fig. 3(a)], the spectrum of the resultant LFP poorly tracked that in tremor-free conditions, and increased power at intermediate frequencies (peaks at 40 and 60 Hz) was noted.

D. Adaptive vs. Static Closed-Loop Control

The closed-loop control scheme was adaptive (i.e., the identification module, RLS in Fig. 2, was run online) to cope with eventual changes in the model population, model mismatches, cellular nonlinearities, and residual dynamics, which could vary across the model populations and the different input amplitudes. To determine the performance advantage of adaptation, a model population was run under tremor conditions but the tremor-locked bursting cells fired bursts at 1 Hz instead of 4 Hz (Section II-C). In that case, the adaptive control scheme quickly updated the model parameters and achieved almost the same performances as in the nominal case (Fig. 8). The control scheme in Fig. 2 was then implemented without the identification module and the functions $F\left(z^{-1}\right)$, $G\left(z^{-1}\right)$, and $H\left(z^{-1}\right)$ were given by (11) with $A\left(z^{-1}\right)$ and $B\left(z^{-1}\right)$ fixed at a nominal value (fixed closed-loop DBS, Fig. 8) previously identified under the tremor condition (4 Hz bursting). In this case, performance quickly declined, compensation in the tremor band was poor, and only a weak restoration of the primary tremor-free rhythm was achieved.

Fig. 9 shows the estimation of the model parameters in $A\left(z^{-1}\right)$ and $B\left(z^{-1}\right)$ at each time step for the adaptive closed-loop scheme used in Fig. 8. Estimated values depended on the actual condition of the model population (i.e., firing patterns of the simulated neurons, tremor cells bursting at ~ 1 Hz) and tracked the changes induced by the stimulation. Both before and during stimulation, the parameter values estimated in steady state conditions (i.e., from 200 and 300 ms, and after 1000 ms, respectively, Fig. 9) differed significantly from the nominal values used for the fixed closed-loop DBS of Fig. 8 (one sample t-test, $p < 0.001$).

Open-loop 130 Hz DBS in Fig. 8 was affected little by the change in the intrinsic dynamics of the model population and provided almost identical results as in Fig. 7(c) and (d). High frequency open-loop DBS overrides the intrinsic dynamics of

the model population and entrains neurons to fire at the stimulation frequency [Fig. 6(d)].

IV. Discussion

This simulation study demonstrates the feasibility of closed-loop control of DBS amplitude to regulate the spectrum of the LFPs, and thereby normalize the aberrant pattern of thalamic neuronal activity present in tremor. We investigated LFPs as the feedback (control) variable as they provide a robust proxy of the overall firing activity of a neural population. The components of the LFP power spectrum depend on the firing pattern of a specific and detectable subset of the neural population [30]–[32] and reflect synchronous activity in populations of neurons [33]. Further, oscillations in the power spectrum of the LFPs at the stimulation site appear to be correlated with the symptoms of movement disorders (e.g., tremor [14], bradykinesia, and rigidity [15], [16]), and modulation of the STN LFP power spectrum at specific frequencies has been noted as a consequence of clinically effective pharmacological therapies [15], [34], STN DBS [16], [32], or the execution of voluntary movements [35]. Further, the strong link between the activity of neurons in the Vim and tremor [18], [36] suggests that LFPs in the Vim would be a reliable marker of the pathological conditions, and that tremor would increase the LFP oscillations in the theta and alpha bands, in agreement with single unit analysis [2], [28]. Conversely, suppression of the LFP oscillations in the theta band would relate to a change in the spiking activity of the tremor cells, which is hypothesized to impact tremor [37].

A. Model Limitations

We used a population of model thalamic neurons, exhibiting the intrinsic firing patterns present in the Vim, to develop and validate the proposed approach to identification and control. In particular, our models were able to generate spike trains whose temporal distribution matched first and second order statistics of the spike trains actually recorded from Vim neurons in tremulous [28] and tremor-free [18], [19] subjects. For simplicity, we employed a point-source approximation of the DBS electrode, and while this appears adequate to represent stimulation [38], the large size of the DBS contact may alter the character of the recorded LFPs. The LFPs were computed by approximating the neuronal membrane as a discrete sequence of point current sources [26], and this created no apparent difference from more detailed approximations [39]. The model included only postsynaptic TC neurons and did not include contributions, either to the LFP or to the evoked neuronal activity, of presynaptic axons and synaptic inputs.

However, the Vim has a low density of neurons and a low level of intranuclear connections (average cellular density: $65\ \mathrm{cell/mm^2}$ [27]). Moreover, as noted previously [23], since DBS activates the axon of TC neurons, which is electrotonically distant from the cell body (where synapses are located), the stimulation effects would be transmitted throughout the network independent of the synapses [21]. Finally, the net effects of synaptic inputs on the firing patterns of TC neurons [18], [28] were carefully reproduced via the intracellular currents applied to generate different patterns of intrinsic activity. However, stimulation could influence the rate and pattern of activity in presynaptic axons and their subsequent synaptic effects on TC cells, and this "indirect" effect of stimulation was not considered. Further, the model was limited to consideration of the effects of DBS on local cells, and downstream network effects (e.g., [40]) were not considered.

B. Identification and Control

A black box approach and linear AR/ARX models were used to describe the relationship between the stimulus (DBS) and response (LFP) and then used for control purposes to restore the features of the reference spectrum. The procedure to identify the models required that the model structure and order were set in advance. Although several criteria (e.g., Akaike information criterion, minimum description length, final prediction error) have been proposed to choose a structure and order for different classes of problems [17], such criteria resulted in model orders higher than the $na = 6,\ nb = 1$ used here. As well, large variability was observed in the (optimal) model order across the different sets of identification/validation data and applied DBS input, but the prediction error was not substantially decreased by the increased model order. The purpose of the model identification was to drive the design of the closed-loop control scheme via a simplified description of the relationship between applied stimuli and LFPs. For that reason, we were not interested in higher order, detailed models, and, since our control scheme targeted the spectral properties of the LFPs, we investigated ARX models that provided sufficient accuracy in prediction of the LFP spectrum. The $na = 6,\ nb = 1$ order was sufficiently low to enable online update of the model parameters, and assured a power spectrum of the one-step ahead prediction that was very close to the actual spectrum (error $\leq 1\%$) independent of the model population (three populations) or location of LFP recording (three different positions for each population). Further indication that the model order and structure were appropriate came from the fitting index proposed by [17]

$$fit = 100\left(1 - \frac{\|y - \hat{y}\|}{\|y - \bar{y}\|}\right)\% \tag{12}$$

where y is any LFP time series to be identified, $\bar{y}$ is its mean value, $\hat{y}$ is the series of one-step ahead predictions produced by a given model, and $\|\cdot\|$ is the norm operator. For each combination of model population and LFP recording position, the proposed ARX model order guaranteed a fit value larger than 96% and the identified transfer functions were similar to those in Fig. 5.

The control input (Fig. 2) was convolved with a train of 100 μs pulses to regulate the stimulation amplitude, while the train frequency (130 Hz) was selected to lie within the effective range of frequencies [5] and to avoid aliasing phenomena in the control signal. The resulting spectra (Fig. 7) showed that the closed-loop DBS restored the primary oscillations observed in the tremor-free condition, but tracking in the gamma band was poor. This was partly due to the choice of the reference signal $r(k)$, which was designed as an average version of the tremor-free LFPs to reduce the effects of the stochastic variability of the neurons and decrease the noise in the evoked potentials. The averaging appeared to amplify the primary oscillation and attenuate the secondary harmonics in the LFPs in the gamma and higher bands. These harmonics, however,

would only subtly affect the movement-related neural signals [31] and, thus, the tracking error may be of minor concern. The closed-loop control system modulated the DBS amplitude based on the feedback information, and was able to adapt to a change in the neuronal oscillation frequency as well as generate a LFP spectrum which approximated the spectrum present in the tremor-free condition much more closely than open-loop fixed intensity stimulation.

The performance of the closed-loop stimulation was remarkably better than that of open-loop stimulation, both at low (20 Hz) and high (130 Hz) frequencies (Fig. 7), suggesting that open-loop stimulation cannot restore the neuronal activity present in tremor-free conditions. This is further supported by experiments [22], [41], showing that random frequency [41] or irregular frequency [22] open-loop DBS, even when delivered at a high average frequency (e.g., 130 Hz), is not effective at relieving tremor.

REFERENCES

[1] S. E. Hua, F. A. Lenz, T. A. Zirth, S. G. Reich, and P. M. Dougherty, "Thalamic neuronal activity correlated with essential tremor," *J. Neurol. Neurosurg. Psychiatry*, vol. 64, pp. 273–276, Feb. 1998.

[2] F. A. Lenz, R. R. Tasker, H. C. Kwan, S. Schnider, R. Kwong, Y. Murayama, J. O. Dostrovsky, and J. T. Murphy, "Single unit analysis of the human ventral thalamic nuclear group: Correlation of thalamic "tremor cells" with the 3–6 Hz component of Parkinsonian tremor," *J. Neurosci.*, vol. 8, pp. 754–764, Mar. 1988.

[3] C. Halpern, H. Hurtig, J. Juggi, M. Grossman, M. Won, and G. Baltuch, "Deep brain stimulation in neurologic disorders," *Parkinsonism Relat. Disord.*, vol. 13, pp. 1–16, Feb. 2007.

[4] E. B. Montgomery and J. T. Gale, "Mechanisms of action of deep brain stimulation (DBS)," *Neurosci. Biobehav. Rev.*, vol. 32, pp. 388–407, Jun. 2008.

[5] A. M. Kuncel, S. E. Cooper, B. R. Wolgamuth, M. A. Clyde, S. A. Snyder, E. B. Montgomery, A. R. Rezai, and W. M. Grill, "Clinical response to varying the stimulus parameters in deep brain stimulation for essential tremor," *Mov. Disord.*, vol. 21, pp. 1920–1928, Nov. 2006.

[6] M. Ushe, J. W. Mink, S. D. Tabbal, M. Hong, P. S. Gibson, K. M. Rich, K. E. Lyons, R. Pahwa, and J. S. Perlmutter, "Postural tremor suppression is dependent on thalamic stimulation frequency," *Mov. Disord.*, vol. 21, pp. 1290–1292, Aug. 2006.

[7] C. Moreau, L. Defebvre, A. Destée, S. Bleuse, F. Clement, J. L. Blatt, P. Krystkowiak, and D. Devos, "STN-DBS frequency effects on freezing of gait in advanced Parkinson's disease," *Neurology*, vol. 71, pp. 80–84, Jul. 2008.

[8] E. Moro, R. J. A. Esselink, J. Xie, M. Hommel, A. L. Benabid, and P. Pollak, "The impact on Parkinson's disease of electrical parameter settings in STN stimulation," *Neurology*, vol. 59, pp. 706–713, Sep. 2002.

[9] A. M. Kuncel, D. A. Turner, L. J. Ozelius, P. E. Greene, W. M. Grill, and M. A. Stacy, "Myoclonus and tremor response to thalamic deep brain stimulation parameters in a patient with inherited myoclonus-dystonia syndrome," *Clin. Neurol. Neurosurg.*, vol. 111, pp. 303–306, Apr. 2009.

[10] E. Moro, P. Piboolnurak, T. Arenovich, S. W. Hung, Y. Y. Poon, and A. M. Lozano, "Pallidal stimulation in cervical dystonia: Clinical implications of acute changes in stimulation parameters," *Eur. J. Neurol.*, vol. 16, pp. 506–512, Apr. 2009.

[11] A. M. Kuncel and W. M. Grill, "Selection of stimulus parameters for deep brain stimulation," *Clin. Neurophysiol.*, vol. 115, pp. 2431–2441, Nov. 2004.

[12] K. J. Åström and B. Wittenmark, *Adaptive Control*, Second ed. Boston, MA: Addison-Wesley, 1995.

[13] L. Rossi, G. Foffani, S. Marceglia, F. Bracchi, S. Barbieri, and A. Priori, "An electronic device for artefact suppression in human local field potential recordings during deep brain stimulation," *J. Neural. Eng.*, vol. 4, pp. 96–106, Jun. 2007.

[14] C. Reck, E. Florin, L. Wojtecki, H. Krause, S. Groiss, J. Voges, M. Maarouf, V. Sturm, A. Schnitzler, and L. Timmermann, "Characterization of tremor-associated local field potentials in the subthalamic nucleus in Parkinson's disease," *Eur. J. Neurosci.*, vol. 29, pp. 599–612, Feb. 2009.

[15] A. A. Kühn, A. Kupsch, G. H. Schneider, and P. Brown, "Reduction in subthalamic 8–35 Hz oscillatory activity correlates with clinical improvement in Parkinson's disease," *Eur. J. Neurosci.*, vol. 23, pp. 1956–1960, Apr. 2006.

[16] N. J. Ray, N. Jenkinson, S. Wang, P. Holland, J. S. Brittain, C. Joint, J. F. Stein, and T. Aziz, "Local field potential beta activity in the subthalamic nucleus of patients with Parkinson's disease is associated with improvements in bradykinesia after dopamine and deep brain stimulation," *Exp. Neurol.*, vol. 213, pp. 108–113, Sep. 2008.

[17] L. Ljung, *System Identification: Theory for the User*, Second ed. Upper Saddle River, NJ: Prentice Hall, 1999.

[18] G. F. Molnar, A. Pilliar, A. M. Lozano, and J. O. Dostrovsky, "Differences in neuronal firing rates in pallidal and cerebellar receiving areas of thalamus in patients with Parkinson's disease, essential tremor, and pain," *J. Neurophysiol.*, vol. 93, pp. 3094–3101, Jun. 2005.

[19] J. Tsoukatos, Z. H. T. Kiss, K. D. Davis, R. R. Tasker, and J. O. Dostrovsky, "Patterns of neural firing in the human lateral thalamus during sleep and wakefulness," *Exp. Brain Res.*, vol. 113, pp. 273–282, Feb. 1997.

[20] J. Haueisen, C. Ramon, M. Eiselt, H. Brauer, and H. Nowak, "Influence of tissue resistivities on neuromagnetic fields and electric potentials studied with a finite element model of the head," *IEEE Trans. Biomed. Eng.*, vol. 44, no. 8, pp. 727–735, Aug. 1997.

[21] C. C. McIntyre, W. M. Grill, D. L. Sherman, and N. V. Thakor, "Cellular effects of deep brain stimulation: Model-based analysis of activation and inhibition," *J. Neurophysiol.*, vol. 91, pp. 1457–1469, Apr. 2004.

[22] M. J. Birdno, S. E. Cooper, A. R. Rezai, and W. M. Grill, "Pulse-to-pulse changes in the frequency of deep brain stimulation affect tremor and modeled neuronal activity," *J. Neurophysiol.*, vol. 98, pp. 1675–1684, Sep. 2007.

[23] A. M. Kuncel, S. E. Cooper, B. R. Wolgamuth, and W. M. Grill, "Amplitude- and frequency-dependent changes in neuronal regularity parallel tremor with thalamic deep brain stimulation," *IEEE Trans. Neural. Syst. Rehabil. Eng.*, vol. 15, no. 2, pp. 190–197, Jun. 2007.

[24] J. Clark and R. Plonsey, "A mathematical evaluation of the core conductor model," *Biophys. J.*, vol. 6, pp. 95–112, Jan. 1966.

[25] N. T. Carnevale and M. L. Hines, *The Neuron Book*. Cambridge, U.K.: Cambridge Univ. Press, 2006.

[26] M. A. Moffitt and C. C. McIntyre, "Model-based analysis of cortical recording with silicon microelectrodes," *Clin. Neurophysiol.*, vol. 116, pp. 2240–2250, Sep. 2005.

[27] C. Hamani, J. O. Dostrovsky, and A. M. Lozano, "The motor thalamus in neurosurgery," *Neurosurgery*, vol. 58, pp. 146–158, Jan. 2006.

[28] M. Magnin, A. Morel, and D. Jeanmonod, "Single-unit analysis of the pallidum, thalamus and subthalamic nucleus in Parkinsonian patients," *Neuroscience*, vol. 96, pp. 549–564, Mar. 2000.

[29] J. Wolfart, D. Debay, G. Le Masson, A. Destexhe, and T. Bal, "Synaptic background activity controls spike transfer from thalamus to cortex," *Nat. Neurosci.*, vol. 8, pp. 1760–1767, Dec. 2005.

[30] P. Brown, A. Oliviero, P. Mazzone, A. Insola, P. Tonali, and V. di Lazzaro, "Dopamine dependency of oscillations between subthalamic nucleus and pallidum in Parkinson's disease," *J. Neurosci.*, vol. 21, pp. 1033–1038, Feb. 2001.

[31] J. F. Marsden, P. Ashby, P. Limousin-Dowsey, J. C. Rothwell, and P. Brown, "Coherence between cerebellar thalamus, cortex and muscle in man: Cerebellar thalamus interactions," *Brain*, vol. 123, pp. 1459–1470, Jul. 2000.

[32] A. Priori, G. Ardolino, S. Marceglia, S. Mrakic-Sposta, M. Locatelli, F. Tamma, L. Rossi, and G. Foffani, "Low-frequency subthalamic oscillations increase after deep brain stimulation in Parkinson's disease," *Brain Res. Bull.*, vol. 71, pp. 149–154, Dec. 2006.

[33] A. A. Kühn, T. Trottenberg, A. Kivi, A. Kupsch, G. H. Schneider, and P. Brown, "The relationship between local field potential and neuronal discharge in the subthalamic nucleus of patients with Parkinson's disease," *Exp. Neurol.*, vol. 194, pp. 212–220, Jul. 2005.

[34] A. Priori, G. Foffani, A. Pesenti, F. Tamma, A. M. Bianchi, M. Pellegrini, M. Locatelli, K. A. Moxon, and R. M. Villani, "Rhythm-specific pharmacological modulation of subthalamic activity in Parkinson's disease," *Exp. Neurol.*, vol. 189, pp. 369–379, Oct. 2004.

[35] C. Brücke, F. Kempf, A. Kupsch, G. H. Schneider, J. K. Krauss, T. Aziz, K. Yarrow, A. Pogosyan, P. Brown, and A. A. Kühn, "Movement-related synchronization of gamma activity is lateralized in patients with dystonia," *Eur. J. Neurosci.*, vol. 27, pp. 2322–2329, May 2008.

[36] S. E. Hua and F. A. Lenz, "Posture-related oscillations in human cerebellar thalamus in essential tremor are enabled by voluntary motor circuits," *J. Neurophysiol.*, vol. 93, pp. 117–127, Jan. 2005.

[37] Z. H. Kiss, D. M. Mooney, L. Renaud, and B. Hu, "Neuronal response to local electrical stimulation in rat thalamus: Physiological implications for mechanisms of deep brain stimulation," *Neuroscience*, vol. 113, pp. 137–143, Aug. 2002.

[38] T. Zhang and W. M. Grill, "Effect of electrode geometry on deep brain stimulation: Monopolar point source vs. Medtroniclead," in *IFMBE Proc. 25th Southern Biomed. Eng. Conf.*, New York, 2009, pp. 167–170.

[39] G. R. Holt and C. Koch, "Electrical interactions via the extracellular potential near cell bodies," *J. Comp. Neurosci.*, vol. 6, pp. 169–184, Mar./Apr. 1999.

[40] J. E. Rubin and D. Terman, "High frequency stimulation of the subthalamic nucleus eliminates pathological thalamic rhythmicity in a computational model," *J. Comput. Neurosci.*, vol. 16, pp. 211–235, May/Jun. 2004.

[41] M. J. Birdno, A. M. Kuncel, A. D. Dorval, A. D. Turner, and W. M. Grill, "Tremor varies as a function of the temporal regularity of deep brain stimulation," *Neuroreport*, vol. 19, pp. 599–602, Mar. 2008.

Sabato Santaniello (S'02–M'08) received the Laurea degree in computer engineering with honors from Università di Napoli Federico II, Napoli, Italy, in 2004, and the Ph.D. degree in information engineering from Università del Sannio, Benevento, Italy, in 2007. In 2006 for one year he was visiting student at the Department of Biomedical Engineering, Duke University, Durham, NC.

He is Postdoctoral Fellow at the Department of Biomedical Engineering, Johns Hopkins University, Baltimore, MD. His research interests include computational neuroscience, modeling and estimation of neural systems, and neural control, with applications to deep brain stimulation.

Giovanni Fiengo (M'02) received the Laurea degree in computer engineering and the Ph.D. degree in information engineering, both from Università di Napoli Federico II, Napoli, Italy, in 1998 and 2001, respectively.

Since 2002, he is Assistant Professor in Automatic Control in the Department of Engineering, Università del Sannio, Benevento, Italy. His research interests are in modeling and control of spark ignition internal combustion engines, three-way catalytic converters, battery modeling and hybrid vehicles, brain cellular modeling and deep brain stimulation.

Luigi Glielmo (S'84–M'90–SM'05) was born in 1960. He received the "laurea" degree in electronic engineering and a research doctorate in automatic control from Università di Napoli Federico II, Napoli, Italy.

He taught at Università di Palermo, at Università di Napoli Federico II and then at Università del Sannio, Benevento, where he is now a Professor of Automatic Control. His current research interests include singular perturbation methods, model predictive control methods, automotive control, DBS modeling and control, power grid optimization. He co-authored more than 100 papers on international archival journals or proceedings of international conferences, and co-edited two books.

Warren M. Grill (S'88–M'95–SM'06) received the B.S. degree in biomedical engineering with honors from Boston University, Boston, MA, in 1989, and the M.S. and Ph.D. degrees, both in biomedical engineering, from Case Western Reserve University, Cleveland, OH, in 1992 and 1995, respectively.

He is Professor of Biomedical Engineering, Neurobiology, and Surgery at Duke University, Durham, NC. His research interests include neural prostheses, design and testing of electrodes and methods for electrical stimulation, the electrical properties of tissues and cells, computational neuroscience, and neural control, with applications to restoration of bladder function, deep brain stimulation, and control of multijoint limb movements. He serves as a Consultant to the Neurological Devices Panel of the Medical Devices Advisory Committee, Center for Devices and Radiological Health, U.S. Food and Drug Administration. He is on the editorial boards of the *Journal of Neural Engineering, Neuromodulation,* and *Medical and Biological Engineering and Computing,* and is Senior Technical Editor for *Neurotech Business Report*.

Dr. Grill is an Associate Editor for the IEEE TRANSACTIONS ON NEURAL SYSTEMS AND REHABILITATION ENGINEERING and Fellow of the American Institute of Biological and Medical Engineering.